INFORMATICS JOURNALS
The Journal of Electrochemical Society of India, Volume 74, Issue (3&4), April – June 2025; pp. 105–115
ISSN (Print) : 0013-466X
ISSN (Online) : xxxx-xxxx
DOI: 10.18311/JESCI/2025/51679

Anti-Corrosion Silica-based Coatings Using Polyelectrolyte Multi-Layered Nanocontainers for Mild Steel

Aarti Gautam[1,2], Ananya Behera[1], K. V. Gobi[2] and R. Subasri[1*]

[1]Centre for Sol-Gel Coatings, International Advanced Research Centre for Powder Metallurgy and New Materials (ARCI), Balapur, Hyderabad – 500005, Telangana State, India

[2]Department of Chemistry, National Institute of Technology, Warangal – 506 004, Telangana State, India

Abstract

Polyelectrolyte multi-layered nanocontainers based on the layer-by-layer deposition method using Fe_2O_3 as the template material were synthesised, where poly (acrylic acid) (PAA) and poly(diallyldimethyl ammonium chloride) (PDADMAC) served as the polyelectrolyte layers. Inorganic corrosion inhibitors, Zr^{4+}, Ce^{3+}, and La^{3+} were sandwiched between the polyelectrolyte layers. The nanocontainers were added to a hybrid silica sol-gel matrix and applied to mild steel substrates. The inhibitor-modified nanocontainer was characterised using an X-ray diffractometer (XRD), Scanning Electron Microscopy (SEM), and zeta potential measurements. The anti-corrosive performance of the developed coatings was analysed using electrochemical impedance spectroscopy, potentiodynamic polarisation studies and salt spray analysis.

Keywords: Corrosion Inhibitor, Mild Steel, Nanocontainers, Polyelectrolyte Multilayers, Silica Coatings

1. Introduction

Metal corrosion is one of the most complex issues to be addressed in recent years, with a particular focus on mild steel corrosion due to its widespread applications in the industrial sector[1]. The most common method to protect metals is through the application of coatings, which avoids the direct contact of the corrosive species with the metal surface[2]. To achieve this, silane films are widely used as they are eco-friendly, cost-effective and are better replacements for hexavalent chrome coating, which is carcinogenic in nature. However, the application of these thin silane films doesn't serve the purpose in the long run. Therefore, to improve the service life of the coating, certain organic or inorganic Corrosion Inhibitors (CIs) are added to the coating matrix[3,4]. According to literature, direct addition of these corrosion inhibitors causes their premature leakage and sometimes may react with the coating matrix, thereby compromising its corrosion protection efficiency[5]. To overcome these challenges, the use of nanocontainers to encapsulate these corrosion inhibitors has been in vogue. These nanocontainers are sensitive to environmental changes in their vicinity, causing the release of CIs to form a passive film on the metal surface, which further delays the corrosion process. According to existing literature, different types of nanocontainers have been reported for encapsulation of CIs, such as Layered Double Hydroxide (LDH)[6], microcapsules[7], Halloysite Nanotubes (HNTs)[8], mesoporous silica[9], Polyelectrolyte Multi-Layer (PML) assembly[10], and zeolite nanoparticles[11]. The choice of nanocontainers depends on certain factors like (1) the type of active agents to be loaded, (2) compatibility with the coating matrix, (3) sensitivity to environmental changes, (4) sustainability, and (5) particle size, which should be small enough to obtain a uniform coating on the metal surface[12].

In our previous work, we have discussed the use of HNTs as nanocontainers to load organic corrosion inhibitor, benzotriazole (BTA)[13] and different inorganic

*Email: subasri@arci.res.in

corrosion inhibitors, Zr^{4+}, La^{3+}, Ce^{3+}, Er^{3+} and Gd^{3+} [14] to protect mild steel surface from corrosion. It was concluded therein that direct addition of inorganic CIs provided better corrosion protection instead of loading them into HNTs. Halloysite nanotubes have inner positively charged alumina layers, which may be the possible reason for the poor loading efficiency of cationic corrosion inhibitors. Therefore, layer-by-layer self-assembly technology may be an alternative for loading cationic corrosion inhibitors in between the oppositely charged polyelectrolyte layers[15].

To the best of our knowledge, there are no reports on the encapsulation of different inorganic CIs into Polyelectrolyte Multi-Layered (PML) nanocontainers (NCs) for developing self-healing coatings on mild steel. Hence, the scope of the current study was to examine the effect of the best-performing inorganic corrosion inhibitors, i.e., Zr^{4+}, La^{3+}, and Ce^{3+}, after they are encapsulated into PML NCs and study their corrosion behaviour in the coating using electrochemical techniques and salt spray test for comparison.

2. Experimental Details

2.1 Materials

3-Glycidoxypropyl trimethoxysilane (GPTMS, Alfa Aesar, Assay-97%) and tetraethylorthosilicate (TEOS, Sigma Aldrich, USA, Assay-98%) precursors were used without further purification, as the starting materials for the synthesis of the organic-inorganic hybrid sol-gel matrix. Polyelectrolyte multi-layered nanocontainers comprising anionic polyacrylic acid (PAA) and cationic polydiallyldimethyl ammonium chloride (PDADMAC) (Sigma Aldrich, USA) were deposited layer-by-layer on in-situ synthesised Fe_2O_3 nanoparticles. cerous nitrate [$Ce(NO_3)_3$] (SRL), lanthanum nitrate [$La(NO_3)_3$] (Alfa Aesar) and zirconyl nitrate [$Zr(NO_3)_4$] (Loba Chemie Pvt Ltd, Mumbai) were used as the source of corrosion inhibitor materials.

Mild Steel (MS) coupons with dimensions of 2.5 cm × 2.5 cm × 0.3 cm were used as substrates for coating generation and characterisation, whereas coupons with dimensions of 5 cm × 2.5 cm × 0.3 cm were used as substrates for salt spray study of coated samples. The chemical composition of mild steel was found to be C: 0.18 wt.%, Mn: 0.58 wt.%, Si: 0.25 wt.%, P:0.018 wt.%, S: 0.037 wt.% and remaining was Fe.

2.2 Synthesis of Iron Oxide Nanoparticles

7 g of $Fe(NO_3)_3.9H_2O$ was dissolved in 40 ml of deionised water (D.I), and 21 g of NaOH was dissolved separately in 100 ml of D.I water. The $Fe(NO_3)_3$ solution was added dropwise to a continuously stirring NaOH solution to form the precipitate of iron hydroxide. The mixture was homogenised for 1 h at 500 rpm, followed by centrifugation. This powder was dried and calcined at 500˚C for 3 h to obtain the iron oxide nanoparticles.

2.3 Synthesis of Inhibitor-Loaded PML Nanocontainer (NC) Powder

1 g of Fe_2O_3 nanoparticles was added to 100 ml of 0.1 M NaCl solution, followed by sonication for proper dispersion of the particles. 0.1 mg/ml of PAA (100 ml) solution was added to the above mixture. The mixture was centrifuged and dried at 80 ºC to obtain the powder. The powder was collected and was re-dispersed in 0.1 M NaCl solution, and then for the deposition of the next layer, 100 ml of $Ce(NO_3)_3$ of concentration 0.0544 g/mL was added to the powder, followed by drying and centrifugation. The above steps were followed for the deposition of the second PAA layer and finally terminated with a polycationic layer, i.e., PDADMAC. After deposition of each layer, the pH of the solution was adjusted to be within 5.5 to 6. The above process was similarly repeated for NCs with $La(NO_3)_3$ (concentration-0.0544 g/mL) and $Zr(NO_3)_4$ (concentration-0.0567 g/mL) as the CIs.

2.4 Sol Synthesis

The procedure for the synthesis of matrix sol was the same as reported in our previous work[13]. To the synthesised matrix sol, 2 wt% of CI-loaded NCs was added and stirred for 2 h. The prepared sols were then used for coating mild steel substrates using the dip-coating technique at a withdrawal speed of 1 mm/s. The coated substrates were cured for 60 min at 130 °C in a drying oven. Figure 1 shows the schematic representation of the experimental procedure involved in the present work.

The nomenclature of different sols along with their details is described in Table 1.

2.5 Characterisation of Nanocontainers

X-ray diffraction (XRD) analysis was carried out on the samples using X-Ray Diffractometer (Bruker AXS D8 Advance, USA) over a wide range of Bragg angles ($5^\circ \leq 2\theta \leq 100^\circ$) with a step size of 0.1˚. Surface morphology and elemental composition of the powder samples were examined

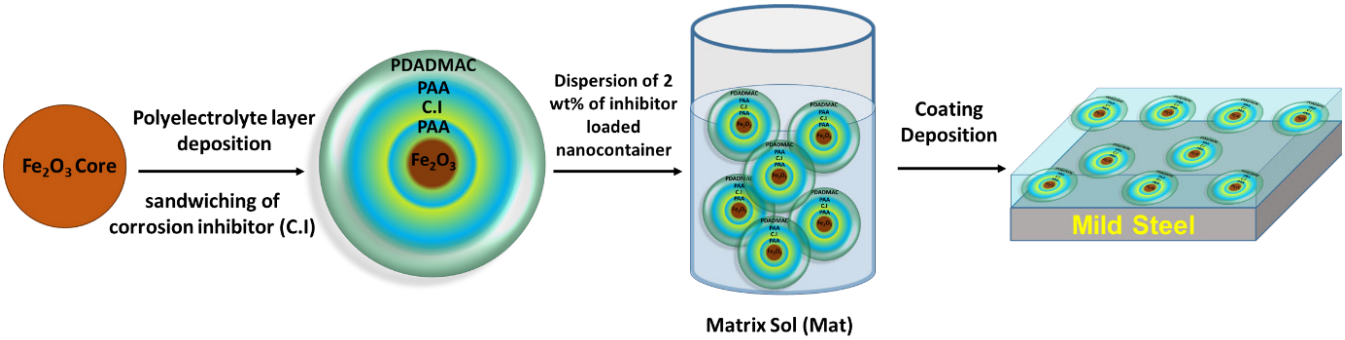


Figure 1. Schematic representation of experimental procedure.

Table 1. Description of sols used for coating the mild steel substrate with their sample ID

S. No.	Description of Sol	Sample ID
1.	Matrix sol	**Mat**
2.	2 wt% of polyelectrolyte multi-layered nanocontainers without corrosion inhibitor	**PML**
3.	2 wt% Zr^{4+}, Ce^{3+}, and La^{3+} - encapsulated nanocontainers and added to matrix sol	**Zr-PML, Ce-PML and La-PML**

using scanning electron microscopy (SEM equipped with EDX spectrophotometer, ZEISS Gemini 500). The Zetasizer (MALVERN AT-0050007) instrument was used to measure the zeta potential of individual layers of PML nanocontainers and to confirm of deposition of the polyelectrolyte layers.

2.6 Characterisation of sols

The viscosity of the sols used for coating application on MS substrates was measured with respect to time to study the shelf life of the sols. The rotational viscometer, Rheolab® QC (Anton Paar, Germany), was used for the measurements.

2.7 Characterisation of Coatings

The thickness of the coated MS substrates was determined using PosiTector® 6000 equipment. An adhesion test was carried out using a multi-hatch gauge BEVS 2203 as per ISO 2409. Coated MS substrates were subjected to salt spray testing as per the ASTM B117 method. The electrochemical analyser from CH Instruments (Model CHI 604E, USA) was used to conduct electrochemical impedance and polarisation studies for uncoated and coated mild steel substrates. A three-electrode electrochemical cell was used to carry out the electrochemical impedance spectroscopy and potentiodynamic polarisation studies, with details as discussed elsewhere[13]. For each coating type, four different measurements (n = 4) were performed. The best-fit data among all the measurements has been reported here.

3. Results and Discussion

3.1 Characterisation of Nanocontainers

Figure 2 (a-h) shows the SEM image and corresponding EDS spectra of Fe_2O_3 nanoparticles (NPs), PML NC powder with Ce^{3+}, La^{3+}, and Zr^{4+} as the CIs, respectively.

It can be observed from the SEM images that after the deposition of polyelectrolyte layers and CI layers onto Fe_2O_3 NPs, the shape of the crystallites has not changed significantly, but the size of the particles has increased from 50 nm to approx. 100 nm. In the case of Zr-PML, the particles appear to be quite larger in size, with an average size above 400 nm. Here, the nanoparticles seem to be covered with a very thin film, which can be due to the reaction of Zr^{4+} with the polyelectrolyte layers. Polyacrylic acid crosslinks with zirconium at the carboxyl groups, forming a durable organic-inorganic composite film (corrosion inhibitors are sandwiched in between two layers of polyacrylic acid)[16]. To confirm the deposition of each consecutive layer, elemental analysis was carried out. For Fe_2O_3 NPs, the presence of Fe and O was evident; for only PML, the major elements were C, O and Fe. For other inhibitor-loaded PML NCs, the constituent CI, i.e., Ce^{3+}, La^{3+} and Zr^{4+}, was present in the Ce-PML, La-PML and Zr-PML NCs, respectively.

Figure 3a shows the XRD pattern of synthesized Fe_2O_3 NPs, only PML, Ce-PML, La-PML, and Zr-PML. XRD

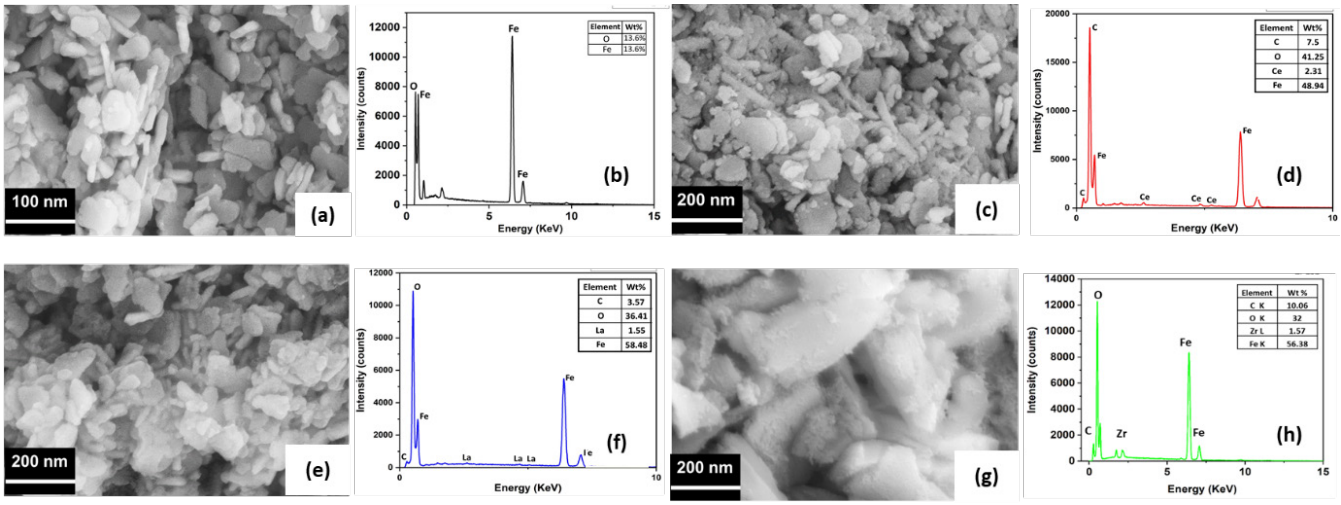


Figure 2. SEM images and EDS spectra **(a and b)** for Fe_2O_3 nanoparticles, **(c and d)** for Ce-PML, **(e and f)** for La-PML, and **(g and h)** for Zr-PML nanopowders.

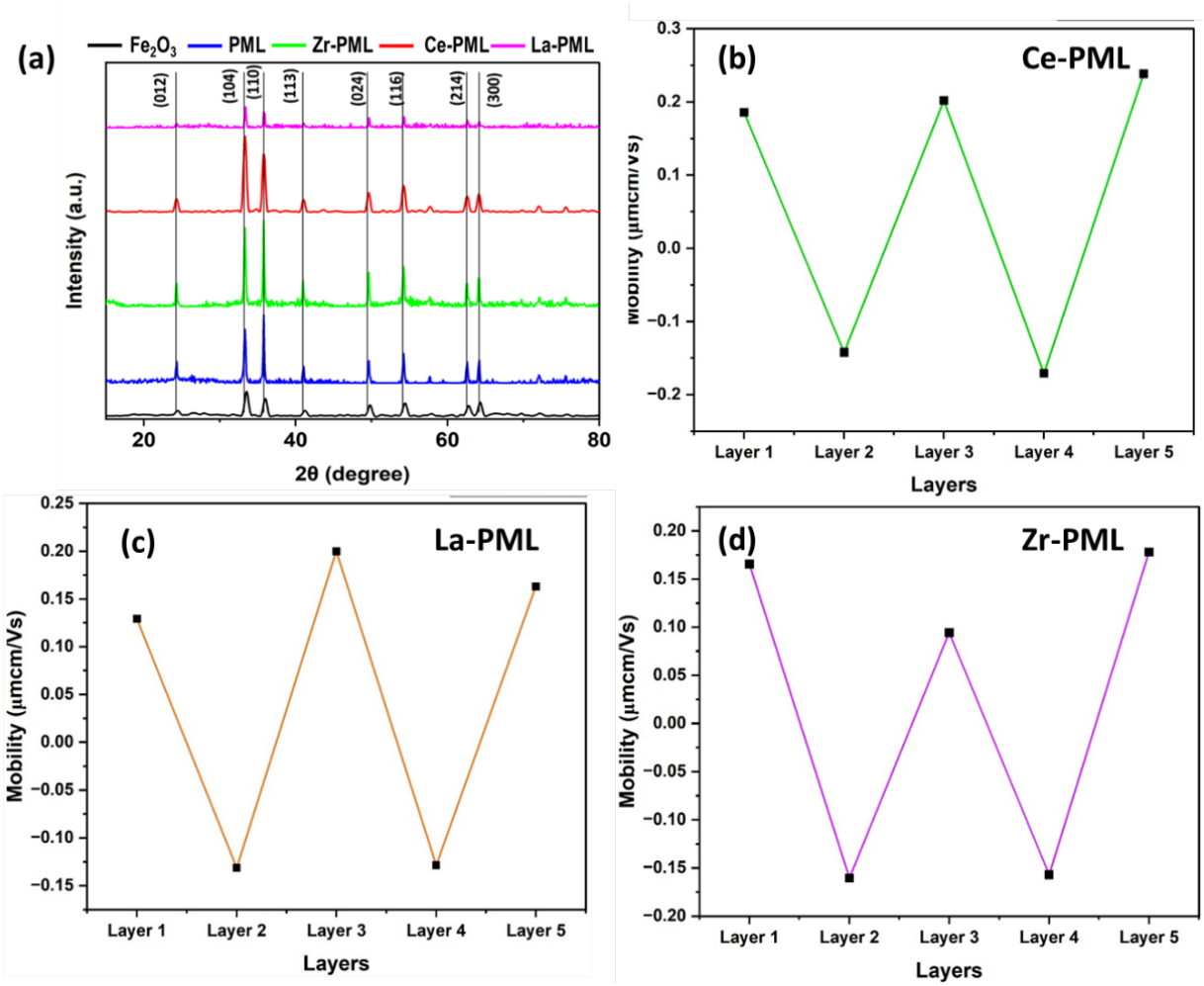


Figure 3. **(a)** XRD pattern of synthesised Fe_2O_3 nanoparticles, only-PML, Ce-PML, La-PML and Zr-PML, and **(b-d)** Electrophoretic mobility data for Ce-PML, La-PML and Zr-PML.

pattern of synthesized Fe_2O_3 NPs shows the diffractions at 2 theta values of 25˚, 32˚, 35˚, 41˚, 50˚, 55˚, 63˚ and 65˚, which correspond to (012), (104), (110), (113), (024), (116), (214) and (300) hkl values, respectively.

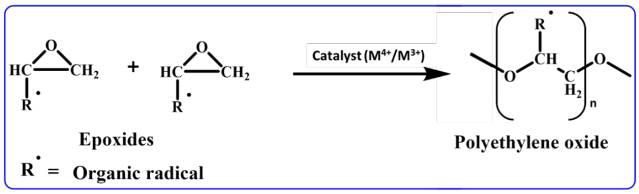
The peak at 32˚ of the 2θ value is the most intense peak, which indicates that the crystal structure of α-Fe_2O_3 was rhombohedral, according to the International Centre for Diffraction Data (ICDD File no. 01-080-5409). The XRD patterns of only polyelectrolyte multi-layered nanocontainers, and PML NC encapsulated with Ce^{3+}, La^{3+} and Zr^{4+} as corrosion inhibitors were analysed. The XRD patterns for all the PML nanocontainers with corrosion inhibitors were similar to that of the iron oxide nanoparticles, suggesting that the inhibitors are well encapsulated in between the layers during the synthesis process and that either the inhibitors (inhibitor oxides) are in an amorphous state or there are no separate crystalline phases of the rare-earth metal oxides at least, within the detection limit of XRD.

Figure 3 (b-d) shows the electrophoretic mobility of different PML confirming the charge associated with each deposited layer.

The zeta potential values of Fe_2O_3 nanoparticles for all layers were observed to be in the range of ±20 to ±40 mV, demonstrating their extreme stability, devoid of any agglomeration. When compared to Ce^{3+} and La^{3+}, the Zr^{4+} particles are less stable, as confirmed by the decrease in the electrophoretic mobility. Zr^{4+} is more likely to exist as free ions as a result of the decreased stability, which also causes poor solubility in the medium. Therefore, deposition of the Zr^{4+}-layer onto the PAA shows poor adherence as seen in Figure. 3 (b-d). In order to confirm this, the viscosity of sols was evaluated with respect to time.

3.2 Viscosity of The Sols

The viscosity of the sols used for coating deposition on MS substrates was measured with respect to time. It is known



Equation 1. Polymerisation of the epoxide functional ring of GPTMS into polyethene oxide.

that metal-based precursors have high catalytic activity for the epoxide ring opening of GPTMS. The epoxide functional group of GPTMS polymerises into polyethene oxide to form a polymer as shown in equation 1[14]. The addition of metal cations can also facilitate Si-O-Si cross-linking in silanes by acting as catalysts for condensation reactions. These metal cations can promote the hydrolysis of silane precursors, leading to the formation of reactive silanol (Si-OH) groups. Subsequently, these groups undergo condensation to form Si-O-Si bonds, enhancing the structural integrity of the silane network[17].

Viscosity data as a function of time for Ce^{3+}, La^{3+}, and Zr^{4+}either added directly or encapsulated into PML nanocontainers, are shown in Figure 4.

From zeta potential measurements, it was clear that among Ce^{3+}, $La^{3+}$and Zr^{4+}, Zr^{4+} ion shows less intercalation between the layers and hence, these ions are free to participate in the hydrolysis/condensation steps of sol-gel synthesis. Interestingly, the viscosity of sols for Zr^{4+}, either when directly added or sandwiched in between the PML NCs, is seen to be nearly the same, confirming that the Zr^{4+} ions are readily available as a catalyst for the polymerisation of the epoxide group. In the case of Ce^{3+} and La^{3+} addition, the increase in the percentage of viscosity with time was substantially higher when directly added as compared to sols with loaded PML NCs. In case of the latter, the sol viscosity is nearly the same as that of the

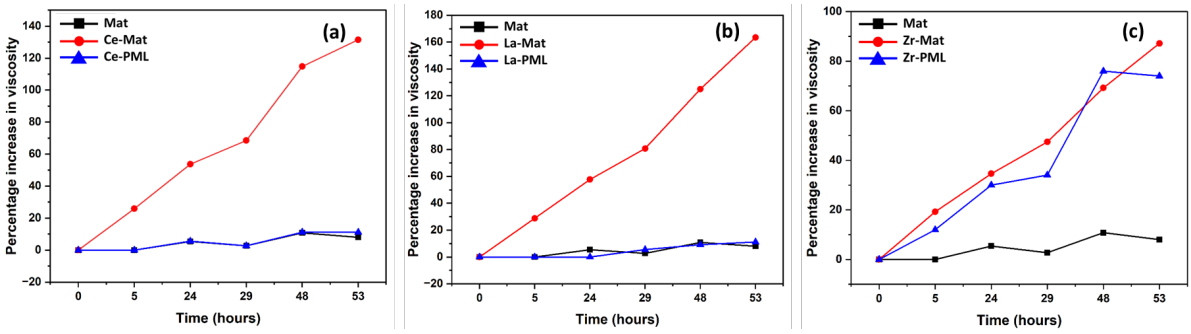


Figure 4. Comparison of the change in viscosity with time for different sols- **(a-c)** Ce, La and Zr-based sols.

matrix sol, thereby confirming that the cationic catalysed polymerisation process either does not take place or takes place at a very negligible rate. From the above, it could be concluded that the observations from zeta potential measurements are in alignment with the viscosity data.

3.3 Coating Characterisation

Figure 5 shows the coating thicknesses obtained for the direct addition of the inorganic inhibitors and PML-based coatings.

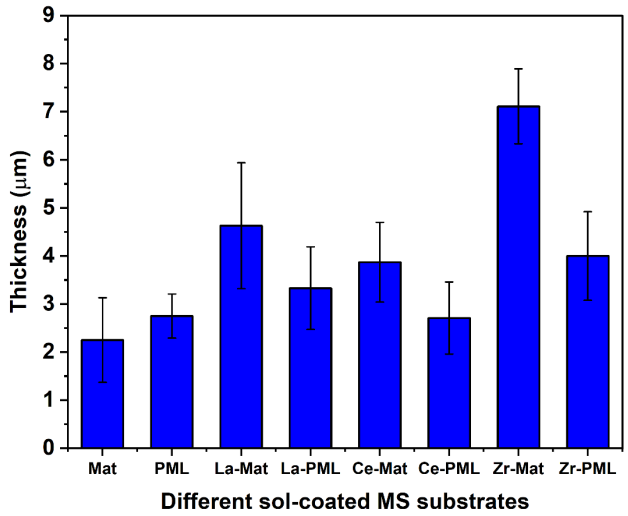


Figure 5. Coating thicknesses of different sol-coated MS substrates.

Although directly adding Zr^{4+} ions into the matrix sol results in the highest coating thickness, zeta-potential and viscosity measurements confirm that these ions remain free when encapsulated within PML NCs. This encapsulation facilitates the polymerisation of the epoxide ring, increasing the sol's viscosity, and thereby enhancing the coating thickness when applied to a mild steel substrate. Similarly, direct incorporation of Ce^{3+} and La^{3+} into the sol produces thicker coatings compared to their encapsulation within PML NCs.

Figure 6 shows the optical microscope images for matrix, PML and Ce-PML coatings before and after the tape peel-off test.

The peel-off adhesion test verified that all the coatings investigated have excellent adhesion and are designated as class 0, i.e., 0% removal or no removal.

3.3.1 Electrochemical Studies

The EIS data were fitted using equivalent electrical circuits as shown in Figure 7 (a) one-time constant for bare substrates and (b) two-time constant for coated substrates. Nyquist plots for different PML NC-based coatings are shown in Figure 7c.

From the EIS data in Figure 7c, it is clear that the impedance for Zr-PML coating was highest with the increase in diameter of the capacitive loop. The corrosion resistance (R_{ct}) values are depicted in the inset of the Nyquist plot. The R_{ct} was highest

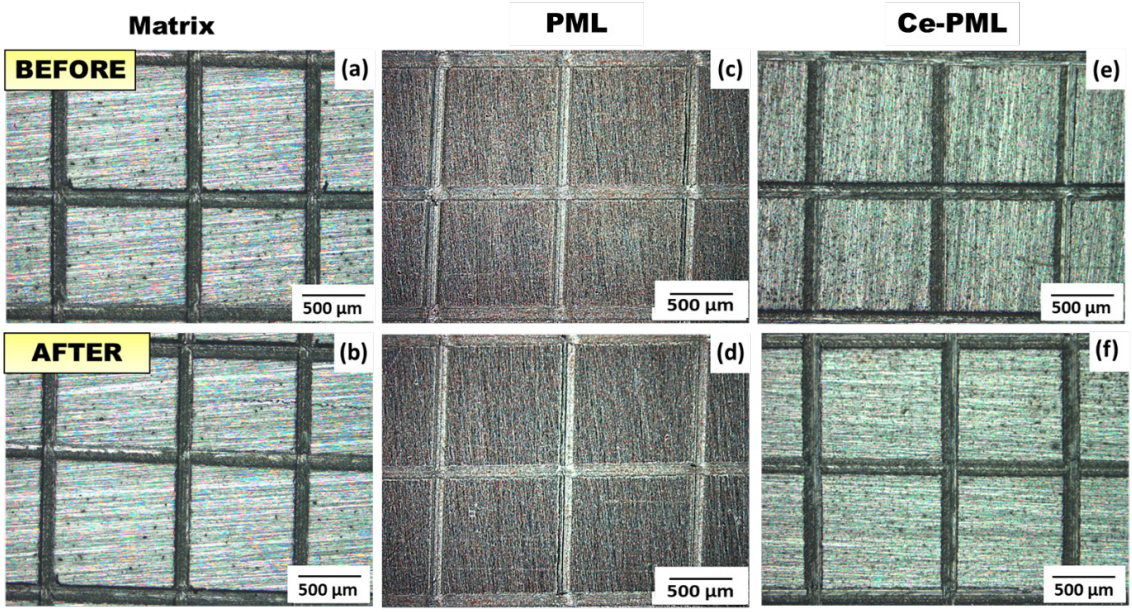


Figure 6. Optical microscope images before and after tape adhesion testing for matrix, PML and Ce-PML coatings.

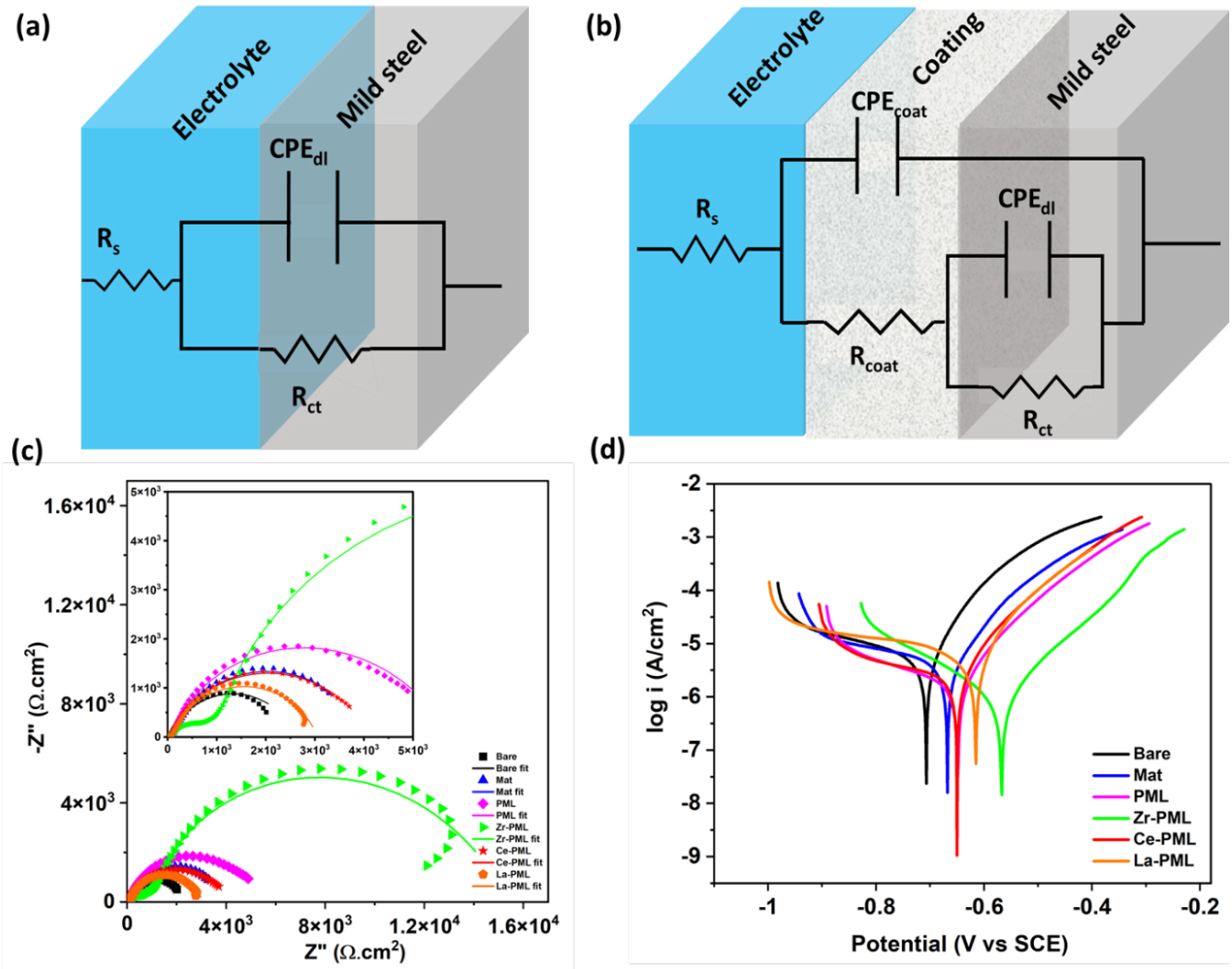


Figure 7. (a and b) Equivalent electrical circuits for bare and coated substrates, and (c and d) Nyquist and polarisation plots for coated and uncoated substrates. Inset of (c) corresponds to a magnified view of the EIS data. The raw EIS data obtained along with the fit data are presented in Figure 7c.

for Zr-PML coating, followed by Ce-PML and then La-PML coatings. To compare the corrosion inhibition properties of PML coatings, the charge transfer resistance and corrosion current density values for the direct addition of C.Is into matrix, i.e., Zirconyl nitrate in matrix sol (Zr-Mat), Cerium nitrate in matrix sol (Ce-Mat), and Lanthanum nitrate (La-Mat) in matrix sol are tabulated in Table 2.

On direct addition, these inorganic or cationic corrosion inhibitors are in close vicinity of any defect and show an immediate reaction to any stimuli caused due to corrosion, thus ensuring quick healing action by forming a stable oxide film on the mild steel surface. The trend of corrosion protection for direct addition and encapsulation is still the same (Zr^{4+} > Ce^{3+} > La^{3+}).

Table 2. Charge transfer resistance and corrosion current density values corresponding to different coatings

Sample	R_{ct}(Ω.cm^2)	I_{corr} (A/cm^2)
Bare	2558	5.54×10^{-6}
Matrix	3813	5.37×10^{-6}
Only-PML	5888	2.18×10^{-6}
Zr-Mat	4.88×10^{7}	1.7×10^{-10}
Ce-Mat	6.10×10^{5}	1.8×10^{-9}
La-Mat	7865	4.57×10^{-6}
Zr-PML	1.42×10^{4}	1.07×10^{-6}
Ce-PML	4090	3.20×10^{-6}
La-PML	2900	3.65×10^{-6}

Similarly, loading or entrapping these corrosion inhibitors into PML NCs reduces their active corrosion inhibition, as the ions responsible for this are not free. With respect to direct addition, the inhibition action of corrosion inhibitor encapsulated into PML NCs follows a similar trend, but with decreased self-healing ability.

Figure 7d shows the polarisation plots for different PML-based coatings. As observed, the corrosion current density for Zr-PML is 1.07×10^{-6} A/cm^2, which is the least among all the coatings, followed by PML with 2.18×10^{-6} A/cm^2. La-PML and Ce-PML coatings have shown nearly the same corrosion current density, but have performed better when compared to bare and matrix-coated mild steel substrates. It is evident from the polarisation curves that the corrosion potential (E_{corr}) for Zr-PML coatings has shifted to a positive potential of -0.58 V, whereas for other coatings it is between -0.60 V to -0.68 V, with bare substrate showing E_{corr} of -0.71 V.

3.3.2 Salt Spray Test

FESEM images along with EDS mapping data were obtained before and after Salt Spray Tests (SST). Figure 8 shows the SST data for only PML and Zr-PML coated substrates, since only the zirconium-based coatings exhibited superior corrosion resistance among the inorganic corrosion inhibitors studied.

EDS maps for PML and Zr-PML coatings at 0 hours showed the complete removal of the coating from the scribe area, with minimal presence of Si and Zr there. However, after 5 hours, the maps revealed the presence of all constituent elements in both the scribe and coated areas, confirming the migration of the corrosion inhibitor to the scribed area and self-healing action through the formation of an oxide film on the exposed surface.

The self-assembly of PML improves the barrier properties of the coating, enabling controlled release of the corrosion inhibitor. During the SST, the polyelectrolyte layers swell due to excessive uptake of NaCl solution, providing a barrier effect for a certain duration and increasing the diffusion path length for chloride ions to penetrate. The role of corrosion inhibitors becomes crucial when the polyelectrolyte layers dissociate or degrade, exposing the CI layer to the corrosive environment and exhibiting self-healing behaviour by forming a passive film. Figure 9 shows the schematic representation of PML coatings on mild steel when immersed in NaCl solution.

The SST results align with the viscosity data and zeta-potential measurements, indicating that Zr-PML sol, being more viscous and having the highest coating thickness, provides enhanced barrier protection and corrosion inhibition.

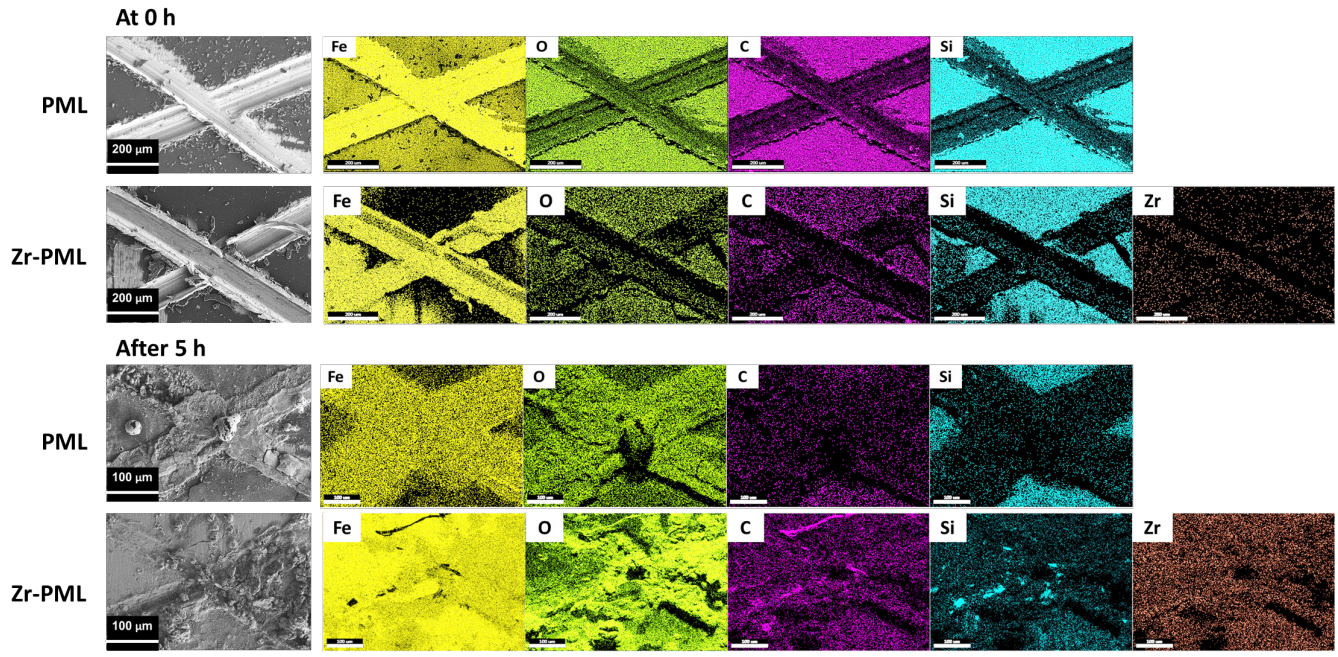


Figure 8. FESEM images before and after salt spray test, along with EDS maps for PML (top) and Zr-PML (bottom) coatings.

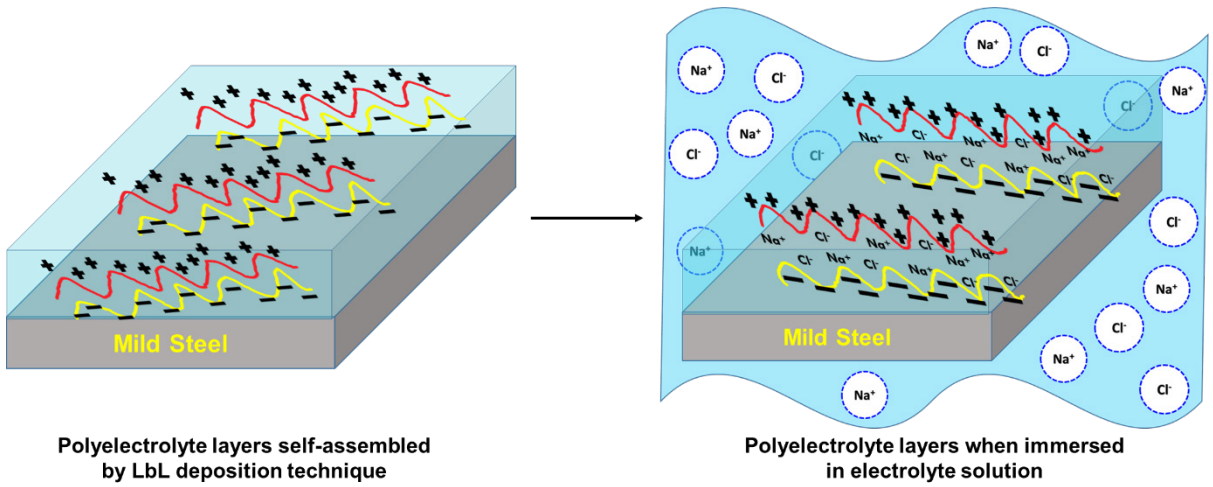


Figure 9. Schematic representation of polyelectrolyte multi-layered coatings when immersed in NaCl solution.

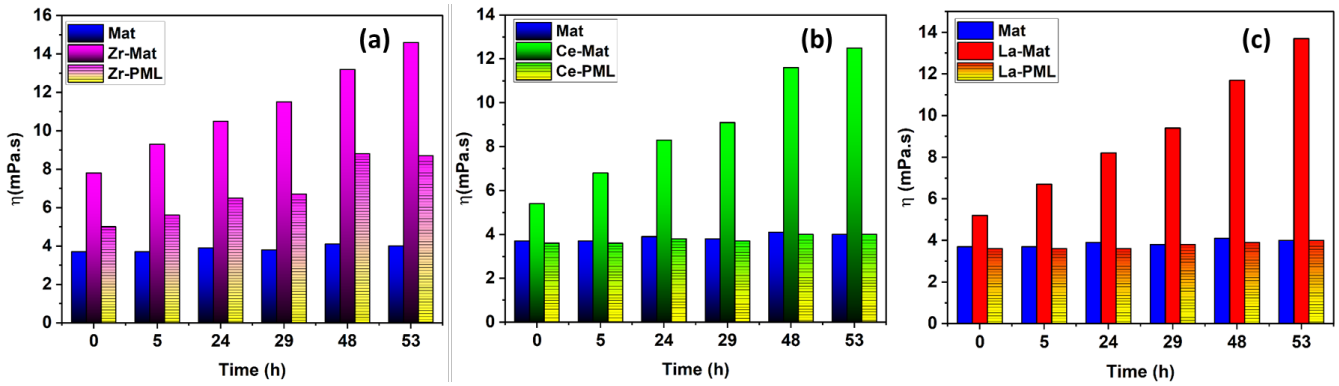


Figure 10. Comparison of the viscosity of different sols when CIs are either added directly or encapsulated into PML NCs into the matrix sol.

3.3.3 Comparison of Data for Direct Addition and After Encapsulating into PML Nanocontainers

Figure 10 shows the comparison of viscosity when corrosion inhibitors were added directly and encapsulated into nanocontainers.

The viscosity of sols for direct addition of corrosion inhibitor increases with an increase in time. On encapsulation into PML nanocontainers, the viscosity for Ce^{3+} and La^{3+} does not increase much when compared to Zr^{4+} encapsulated into PML nanocontainers or with direct addition to the matrix, which may be due to entrapment of these cationic CI, which prevents their reaction with the matrix sol. The ionic radius for Zr^{4+} is 80 pm, whereas for Ce^{3+} and La^{3+} the ionic radius is 102 and 103 pm, respectively. As per ionic radius, the particle size of Zr^{4+} ions is very likely to effectively intercalate into the polyelectrolyte layers and thus they exist in the form of free ions, which are readily available to react with the matrix sol, thereby increasing the sol viscosity.

Figure 11 shows the comparison of charge transfer resistance data obtained after fitting the electrochemical impedance data.

Based on the R_{ct} data, it can be observed that coatings from the direct addition of CI exhibit the highest charge transfer resistance when compared to PML-based coatings. When compared to matrix-coated substrates, Ce-PML coatings demonstrate a negligible increase in R_{ct} values, while La-PML coatings provide more or less similar protection as bare Mild Steel (MS) substrates. The above data confirms that the coatings developed by the direct addition of CIs impart excellent barrier effect, probably due to the higher coating thickness obtained from ring opening and polymerisation of the epoxide group, which could be substantiated from the viscosity

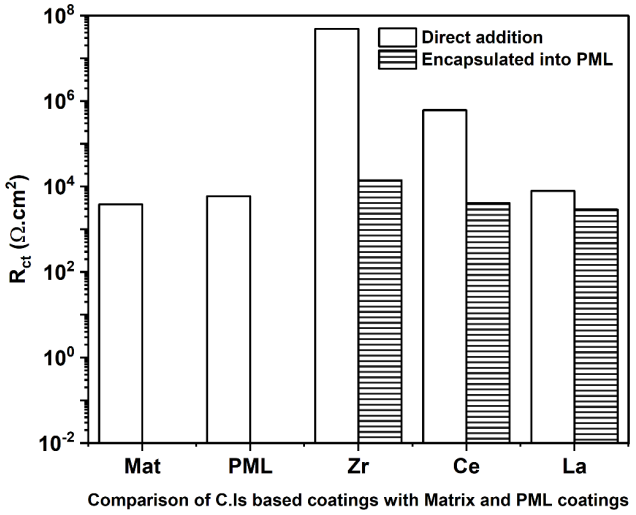


Figure 11. Comparison of charge transfer resistance of coatings using different nanocontainers (NCs) encapsulating different inorganic corrosion inhibitors.

Table 3. Comparison of normalised charge transfer resistance with respect to the coating thickness for different coatings

CSample	R_{ct}(Ω.cm²)	Thickness (µm)	Normalized R_{ct}(Ω.cm²)
Zr-Mat	4.88×10^7	7.11	6.86×10^6
Ce-Mat	6.10×10^5	3.87	1.57×10^5
La-Mat	7.86×10^3	4.63	1.69×10^3
Zr-PML	1.42×10^4	4.00	3.55×10^3
Ce-PML	4.09×10^3	2.71	1.51×10^3
La-PML	2.90×10^3	3.33	8.71×10^2

data also. Higher coating thickness results in higher barrier property, which in turn slows down the corrosion process at the coating-metal interface. To delineate the effect of thickness and determine only the inhibitory effect of the cationic corrosion inhibitors, a normalised Rct was calculated by determining the ratio of R_{ct} and thickness, assuming the coating to be uniform with respect to thickness and presented in Table 3.

The normalised R_{ct} for direct addition of corrosion inhibitors exhibits enhanced corrosion protection relative to their addition into polyelectrolyte multi-layered nanocontainers. For instance, the Zr-Mat coatings demonstrated threefold corrosion protection compared to Zr-PML coatings, as seen from the normalised R_{ct} values where thickness effects are delineated. For the short duration of exposure to corrosion medium, direct addition of corrosion inhibitors into the coating matrix provides high corrosion resistance, when compared to encapsulation and addition to the coating matrix. However, further studies are planned to investigate the long-term effects of encapsulating the C.I. into the PML NCs.

The present investigation confirmed that the encapsulation of inorganic corrosion inhibitors may not be efficient if any immediate action is required. But on comparing our data with the present work going on around the world confirm that coatings developed using inorganic CIs on mild steel are capable enough to withstand aggressive environmental conditions, such as salt spray and show active inhibition action during electrochemical studies. Li *et al.*[18] in their work reported the use of mesoporous silica particles as a core onto which a layer of mercaptobenzothiazole (MBT) was deposited, followed by deposition of polyelectrolyte layers. The developed nanocontainer was added to the silane solution, and a coating was applied to carbon steel. The data reveal that the i_{corr} values for coatings based on loaded nanocontainers after 1 h immersion into 3.5 wt% NaCl were 3.02×10^{-6} A/cm². Similarly, Fouda *et al.*[19] in their work reported the electrochemical data after immersing mild steel substrates in a chloride solution of La^{3+} and Sm^{3+} for 30 min. The i_{corr} values for the maximum concentration of inhibitor in the solution, i.e., 0.4 g/L, were 14.63×10^{-6} A/cm² for lanthanum chloride and 9.42×10^{-6} A/cm² for samarium chloride, respectively. Hence, it is clear that i_{corr} values for the above-reported literature are comparatively higher with respect to our coating (Z-PML), which shows an i_{corr} value of 1.07×10^{-6} A/cm², confirming its active inhibition action.

4. Conclusions

i. Viscosity of sols based on direct addition of cationic corrosion inhibitors to the sol-gel matrix was higher when compared to adding after loading them into nanocontainers. The metal-cations initiate epoxide ring opening of GPTMS, and in addition, they accelerate the Si-O-Si cross-linking, increasing the sol viscosity and thereby increasing the thickness of the coating. Catalytic activity of Zr^{4+} was seen to be higher than Ce^{3+} and La^{3+} about epoxide ring opening, and hence, coating thickness of Zr^{4+} based coatings was seen to be highest, followed by Ce^{3+} and then La^{3+}.

ii. The charge transfer resistance of Zr-PML coating was 1.42×10^4 **Ω.cm²**, which is higher than that of

the Ce-PML and La-PML coatings, i.e., 0.41 × **10^4 Ω.cm**^{2} and 0.29 × **10^4 Ω.cm**^{2}, respectively. Zr^{4+} is a better cationic inhibitor than Ce^{3+} and La^{3+}, which could be discerned from the thickness-independent normalised R_{ct} values given in Table 3

iii. The encapsulated Zr^{4+} in PML NC showed higher corrosion resistance and lower corrosion rate when compared to Ce^{3+} in PML NC and La^{3+} in PML NC coatings.

iv. Salt spray test revealed that the coatings based on CIs encapsulated into PML NC show excellent barrier and inhibition properties, when compared to bare MS or only PML (PML NC without CI) coatings.

5. References

1. Wu Y, Duan Y, Qiu J, Gao X, Ma H. A pH-responsive intelligent coating based on composite CaCO3 microspheres for long-term corrosion protection of Q235 carbon steel. Appl Surf Sci. 2022; 578, 151980. https://doi.org/10.1016/j.apsusc.2021.151980
2. Cao Y, Yuan X, Wang X, Wu H, Wang G, Yang H. Improving the self-healing performance of the water-borne epoxy anticorrosion coating in 3.5 wt% NaCl solution using acid and alkaline dual sensitive organic microspheres. Prog Org Coat. 2022; 167, 106815. https://doi.org/10.1016/j.porgcoat.2022.106815
3. Chen Y, Lu X, Lamaka SV, Ju P, Blawert C, Zhang T, *et al.* Active protection of Mg alloy by composite PEO coating loaded with corrosion inhibitors. Appl Surf Sci. 2020; 504, 144462. https://doi.org/10.1016/j.apsusc.2019.144462
4. da Silva RMP, Izquierdo J, Milagre MX, Antunes RA, Souto RM, Costa I. Development of an Al3+ ion-selective microelectrode for the potentiometric microelectrochemical monitoring of corrosion sites on 2098-T351 aluminium alloy surfaces. Electrochim Acta. 2022; 415, 140260. https://doi.org/10.1016/j.electacta.2022.140260
5. Sun D, Yan Z, Mingzhang L, Ziming W, Suping C, Yang J. Robust and impermeable metal shell microcapsules for one-component self-healing coatings. Appl Surf Sci. 2021; 546, 149114. https://doi.org/10.1016/j.apsusc.2021.149114
6. Alibakhshi E, Ghasemi E, Mahdavian M, Ramezanzadeh B. A comparative study on corrosion inhibitive effect of nitrate and phosphate intercalated Zn-Al-Layered Double Hydroxides (LDHs) nanocontainers incorporated into a hybrid silane layer and their effect on cathodic delamination of epoxy topcoat. Corros Sci. 2017; 115, 159-74. https://doi.org/10.1016/j.corsci.2016.12.001
7. Song YK, Lee TH, Lee KC, Choi MH, Kim JC, Lee SH, *et al.* Coating that self-reports cracking and healing using microcapsules loaded with a single AIE fluorophore. Appl Surf Sci. 2020; 511, 145556. https://doi.org/10.1016/j.apsusc.2020.145556
8. Jiang J, Sun Y, Chen Y, Zhou Q, Rong H, Hu X, *et al.* Ultrasonic-assisted Ni-Mo-P doping hydrothermal synthesis of clustered spherical MoS2 composite coating: wear and corrosion resistance. Surf Eng. 2020; 36(8), 889-99. https://doi.org/10.1080/02670844.2020.1726012
9. Xie ZH, Li D, Skeete Z, Sharma A, Zhong CJ. Nanocontainer-enhanced self-healing for corrosion-resistant Ni coating on Mg alloy. ACS Appl Mater Interfaces. 2017; 9(41), 36247-60. https://doi.org/10.1021/acsami.7b12036
10. Yang G, Ma H, Yu L, Zhang P. Preparation and characterisation of layer-by-layer self-assembled polyelectrolyte multilayer films doped with surface-capped SiO2 nanoparticles. J Colloid Interface Sci. 2009; 333(2), 776-81. https://doi.org/10.1016/j.jcis.2009.02.024
11. Zhou C, Li Z, Li J, Yuan T, Chen B, Ma X, *et al.* Epoxy composite coating with excellent anticorrosion and self-healing performances based on multifunctional zeolitic imidazolate framework-derived nanocontainers. Chem Eng J. 2020; 385, 123835. https://doi.org/10.1016/j.cej.2019.123835
12. Jiang J, Chen H, Wang Y, Zhu L, Sun Y, Lin H, *et al.* Effect of ultrasonication and Na2MoO4 content on properties of electroless Ni-Mo-P coatings. Surf Eng. 2019; 35(10), 873-82. https://doi.org/10.1080/02670844.2018.1537612
13. Gautam A, Soma Raju KRC, Gobi KV, Subasri R. Capped inhibitor-loaded halloysite nanoclay-based self-healing silica coatings for corrosion protection of mild steel. Ceram Int. 2022; 48(20), 30151-63. https://doi.org/10.1016/j.ceramint.2022.06.288
14. Gautam A, Soma Raju KRC, Gobi KV, Subasri R. Effect of transition metal and different rare-earth inhibitors-based sol-gel coatings on corrosion protection of mild steel. Met Mater Int. 2023; 29(10), 2909-25. https://doi.org/10.1007/s12540-023-01426-6
15. Kamburova K, Boshkova N, Boshkov N, Radeva T. Design of polymeric core-shell nanocontainers impregnated with benzotriazole for active corrosion protection of galvanised steel. Colloids Surf A Physicochem Eng Asp. 2016; 499, 24-30. https://doi.org/10.1016/j.colsurfa.2016.03.067
16. Hatanaka K, Fukui M, Mukai Y, Toyose K. Coating adhesion and corrosion resistance of polyacrylic acid-zirconium composite-treated aluminium. J Light Met. 1990; 40(1), 1-7. https://doi.org/10.2464/jilm.40.1
17. Suegama PH, de Melo HG, Benedetti AV, Aoki IV. Influence of cerium (IV) ions on the mechanism of organosilane polymerisation and on the improvement of its barrier properties. Electrochim Acta. 2009; 54(9), 2655-62. https://doi.org/10.1016/j.electacta.2008.11.007
18. Li L, Jiang J, Hans S. Preparation of intelligent corrosion-resistant coatings based on pH-responsive silica nanocontainers. Microporous Mesoporous Mater. 2023; 349, 112418. https://doi.org/10.1016/j.micromeso.2022.112418
19. Fouda AS, Abd el-Wahab SM, Attia MS, Youssef AO, Elmoher HO. Rare-earth metals as eco-friendly corrosion inhibitors for mild steel in produced water. Der Pharma Chem. 2015; 7(3), 74-87. Available from: http://derpharmachemica.com/archive.html